ASSESSMENT OF WATER ICE AT THE LUNAR NORTH POLE BASED ON LROC NARROW ANGLE CAMERA IMAGERY AND MINI-RF RADAR DATA. J. L. Mitchell[1], S. J. Lawrence[1], E. J. Speyerer[1], M. S. Robinson[1], and B. W. Denevi[2], [1]School of Earth and Space Exploration, Arizona State University, Tempe, AZ. (Julie.L.Mitchell@asu.edu), [2]Johns Hopkins University Applied Physics Laboratory, Laurel, MD.

Introduction: Permanently shadowed regions (PSRs) at the lunar poles are high-priority exploration targets because they may provide a reservoir of exploitable volatiles [**1-4** and others**]**. Since PSRs receive little solar insolation they exhibit annual average temperatures lower than the sublimation temperature of H_2O (~104K), allowing them to trap water and other volatiles over time [**1**]. Despite numerous remote sensing experiments the grade and tonnage of these putative deposits is still unknown. The purpose of this study is to investigate the presence of volatiles in lunar PSRs using radar and visible imagery.

Background: The Lunar Reconnaissance Orbiter (LRO) Mini-RF instrument actively transmitted circularly-polarized S-band (12.6-cm) radar waves [**5**]. Studies to date have found that some polar PSR craters exhibit abnormally high circular polarization ratios (CPRs) in their interiors surrounded by low CPR signatures [**6**]. These CPR anomalies are hypothesized to be due to the presence of water ice deposits in the PSRs [**6**]. S-band radar is sensitive to ice deposits at the wavelength scale because they result in double-bounce backscatter; however, S-band is also sensitive to blocks at the wavelength scale. The presence or absence of blocks needs to be assessed as an alternative to the ice hypothesis. The Lunar Reconnaissance Orbiter Camera (LROC) Narrow Angle Camera (NAC) is obtaining meter scale observations of illuminated potions of the poles [**7, 8**]. Long-exposure NAC imagery reveals the interiors of PSRs, allowing a quantitative assessment of blocks in PSRs.

Methods: A qualitative distribution of double-bounce backscatter detected by Mini-RF can be generated using the *m-chi* decomposition. This technique [**9**] separates radar returns into single-bounce (Bragg) backscatter indicative of features smooth at the wavelength scale, volume scattering such as from lunar regolith, and double-bounce backscatter. *M-chi* decomposition can be displayed as a colorized map, where Bragg scattering is green, volume scattering blue, and double-bounce backscatter red [9] (**Fig. 1**).

LROC long-exposure NAC images are used for two purposes in this study: 1) to determine the boundaries of PSRs, and 2) to allow a quantitative comparison of blocks between regions with potentially high concentrations of ice, and regions without ice. Long-exposure images of PSRs have larger pixel scales than nominal-exposure products (10-20 m/px versus 0.5-1.0 m/px nominal); therefore, only blocks larger than 20-40 m in diameter can be detected in PSRs. *M-chi* maps and block counts were produced for four CPR-anomalous craters and two CPR-normal craters at the north pole, and two CPR-anomalous equatorial craters (**Table 1**).

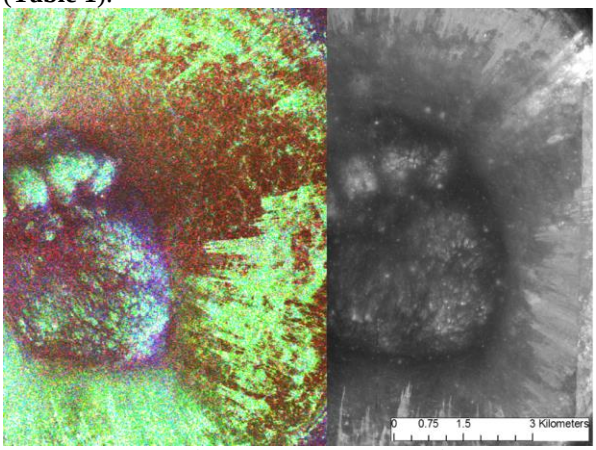

Fig. 1. M-chi map (left) and LROC NAC (right) of CPR-anomalous equatorial crater Gardner.

Table 1. Craters included in this study.

Crater	Lat (°N)	Long (°E)	CPR	Age
Rozhdestvensky N	84.04	203.73	Anom.	Imbrian
Lovelace E	82.04	263.22	Anom.	Imbrian
Lovelace	82.08	250.49	Anom.	Imbrian
Whipple	89.14	120.05	Anom.	pre-Nectarian
Main L	81.44	22.73	Normal	Copernican
Plaskett U	82.41	162.29	Normal	Eratosthenian
Byrgius C	21.17	295.49	Anom.	Copernican
Gardner	17.73	33.80	Anom.	Imbrian

Using the standard LROC processing pipeline [**7**] and CraterTools [**10**], block size-frequency distributions (SFDs) were produced at craters with multiple observed blocks. The slope of the log-log plot of the SFD, known as *B* from [**11**], allows a comparison of the block size distribution between CPR-anomalous polar and equatorial craters. If polar CPR-anomalous craters have *B* values statistically distinct from CPR-anomalous equatorial craters (which cannot have ice due to high annual temperatures), then there must be differences between the physical properties of the crater interiors between the polar and nonpolar regions.

Results: *M-chi* decompositions for each of the craters listed in Table 1 were produced. Rozhdestvensky N showed pervasive double-bounce backscatter in its interior and no visible blocks (**≥**20 m diameter). Other craters where the presence of ice was proposed [**3**] were dominated by Bragg scattering with patches of

double-bounce backscatter and contained <0.2 blocks per km^2. The low quantity of visible blocks could be the result of resolution limitations since the majority of visible blocks in equatorial crater interiors were <15 m in diameter (**Fig. 2**).

Only four craters had enough blocks to generate SFDs and be compared for trends in block sizes and frequencies (**Table 2**). If block SFDs were significantly different between CPR anomalous and CPR normal craters, then *B* values could potentially be used to distinguish roughness from water ice. However, as Table 2 shows, the *B* values were not significantly different between the two populations of craters, showing that block populations do not correlate with radar backscatter properties in these few cases.

Table 2. B value results. Shaded boxes indicate no B value due to a lack of visible blocks. *Values from [12] for comparison.

Crater	Candidate for Ice?	B Values	
		Interior	Exterior
Rozhdestvensky N	Yes		
Lovelace E	Yes		-3.62
Lovelace	Yes		-4.98
Whipple	Yes	-3.44	-0.93
Main L	No	-3.17	-3.06
Plaskett U	No		
Byrgius C	No	-5.5	-6.05
Gardner	No	-2.84	-3.5
Surveyor I*	No	-3.29*	-3.93*
Surveyor III*	No	-4.93*	-6.12*
Surveyor VI*	No	-4.23*	-3.52*

Block densities as a function of age were also explored using published ages [**6, 13**] for each of the craters studied. Because younger craters have not been exposed to meteorite bombardment as much as older craters, they should contain higher numbers of blocks in both their interiors and exteriors [**14**]. While a general decrease in the density of ejecta blocks was seen with age, several young polar craters were outliers because they did not contain blocks in their interiors or exteriors.

Discussion: *M-chi* decompositions of polar CPR-anomalous craters showed a range of double-bounce backscatter in their PSRs. Rozhdestvensky N is the most likely crater in this study to harbor ice deposits because it had the highest double-bounce signature and no visible blocks (at 20 m scale). Other craters contained patches of double-bounce backscatter, and these patches may be regions with ice deposits or hidden, sub-surface clasts. The low double-bounce backscatter does not necessarily preclude the presence of water ice. Ice diffused within the regolith could be present, but undetectable by current remote sensing methods. Block counts show similar block sizes and densities between CPR-normal polar and CPR-anomalous equatorial craters. There is no statistically-significant variation in *B* values between all types of craters, preventing that metric from being a distinguishing factor between crater types.

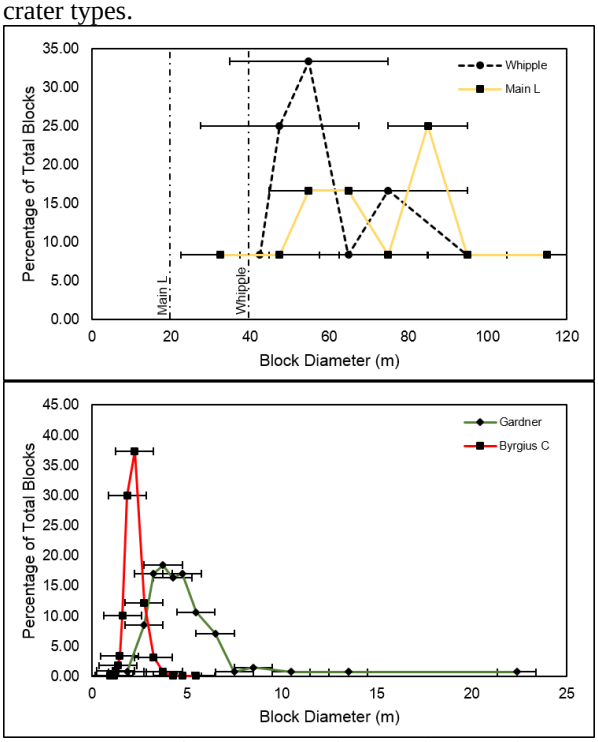

Fig. 2. Percentage of total blocks as a function of diameter for crater interiors. Top: PSR interiors from long-exposure imagery (10-20 m pixel scales); bottom: equatorial craters nominal-exposure imagery.

Conclusions: Block counts and SFDs did not reveal substantial differences between CPR-anomalous and CPR-normal polar craters. The lack of consistent double-bounce backscatter in potential ice-bearing PSRs in this study indicates one of two possibilities: 1) not all lunar PSRs have water ice, or 2) there is water ice, but the physical state of the deposits does not lend itself to detection through analyses of this type. Future work should include *m-chi* maps and block counts of other polar CPR-anomalous craters, including south pole PSRs that are generally larger than PSRs at the north pole.

References: [1] Paige, D. A. et al. (2010a) *Sci, 330, 479-482.* [2] Sanin, A. et al. (2012) *JGR, 117.* [3] Lucey, P. et al. (2014) *JGR-P, 119, 1665-1679.* [4] Colaprete, A. et al. (2010) *Sci., 330, 463.* [5] Raney, R. K. et al. (2011), *IEEE, 99, 808*-823. [6] Spudis, P. D., et al. (2013) *JGR-P, 118, 2016-2029.* [7] Robinson, M. S. et al. (2010), *Sp. Sci. Rev., 150, 81-124.* [8] Koeber, S. D. et al. (2014) *LPS XLV*, Abst. # 2811. [9] Raney, R. K. et al. (2012) *JGR-P, 117.* [10] Kneissl, T. S. et al. (2011) *Plan. Sp. Sci., 59, 1243-1254.* [11] Hartmann, W. K. (1969) *Icarus, 10, 201-213.* [12] Cintala, M. J. and McBride, K. M. (1994) *NASA Tech. Mem. 104804.* [13] Lucchitta, B. (1978) *USGS, Map, I-1062.* [14] Hapke, B. (1973) *Moon, 7, 342-355.*